
Augmented Random Search for Multi-Objective Bayesian Optimization of Neural Networks

Mark Deutel

Friedrich-Alexander-Universität
Erlangen, Germany
mark.deutel@fau.de

Georgios Kontes

Fraunhofer Institute for Integrated Circuits IIS
Nürnberg, Germany
georgios.kontes@iis.fraunhofer.de

Christopher Mutschler

Fraunhofer Institute for Integrated Circuits IIS
Nürnberg, Germany
christopher.mutschler@iis.fraunhofer.de

Jürgen Teich

Friedrich-Alexander-Universität
Erlangen, Germany
juergen.teich@fau.de

Abstract

Deploying Deep Neural Networks (DNNs) on tiny devices is a common trend to process the increasing amount of sensor data being generated. Multi-objective optimization approaches can be used to compress DNNs by applying network pruning and weight quantization to minimize the memory footprint (RAM), the number of parameters (ROM) and the number of floating point operations (FLOPs) while maintaining the predictive accuracy. In this paper, we show that existing multi-objective Bayesian optimization (MOBOpt) approaches can fall short in finding optimal candidates on the Pareto front and propose a novel solver based on an ensemble of competing parametric policies trained using an Augmented Random Search Reinforcement Learning (RL) agent. Our methodology aims at finding feasible tradeoffs between a DNN’s predictive accuracy, memory consumption on a given target system, and computational complexity. Our experiments show that we outperform existing MOBOpt approaches consistently on different data sets and architectures such as ResNet-18 and MobileNetV3.

1 Introduction

The deployment of DNNs on tiny devices is restricted to the constraints imposed by the target platform. Constraints such as <1MB Flash, <512Kb RAM, and clock speeds in the low MHz range make the design of DNN models for such platforms challenging. In general, several conflicting objectives and constraints such as memory availability, inference time, and power consumption of the deployed DNN model must be considered.

This work investigates multi-objective Bayesian optimization (MOBOpt) of DNN hyperparameters for embedded devices (such as ARM Cortex-M platforms) using deep compression. The goal of multi-objective optimization (MOOpt) is to either maximize or minimize a set of objectives. Assume, without loss of generality, maximizing some set of objective functions $f(x) = [f_1(x), \dots, f_n(x)] \in \mathbb{R}^n$, where $n \geq 2$, while satisfying a set set of constraints $g(x) \geq 0 \in \mathbb{R}^V$ where $V \geq 0$, $x \in \mathcal{X} \subset \mathbb{R}^d$, and \mathcal{X} is a compact set. Usually, there exists no single solution x^* that maximizes all objectives while also satisfying all V constraints.

Definition 1.1. [6] An objective function evaluation $f(x)$ *Pareto-dominates* $f(x')$, denoted as $f(x) \succ f(x')$, if $f_m(x) \geq f_m(x')$ for all $m = 1, \dots, M$ and there exists at least one $m \in \{1, \dots, M\}$ such that $f_m(x) > f_m(x')$.

Definition 1.2. [6] A set of Pareto-optimal tradeoffs $\mathcal{P}(x)$ over a set of samples $X \subseteq \mathcal{X}$ is called the *Pareto front* (PF).

$$\mathcal{P}(X) = \{f(x) : x \in X, \nexists x' \in X \text{ s.t. } f(x') \succ f(x)\}$$

$\mathcal{P}_{feas}(X) = \mathcal{P}(\{x \in X : g(x) \geq 0\})$ is defined as the *feasible PF*.

Hence, the goal of MOOpt is to identify an approximate PF $\mathcal{P}(X_n)$ of the true PF $\mathcal{P}(X)$ within a search budget of n evaluations. For problems where the true Pareto-front is not known, the quality of $\mathcal{P}(X_n)$ is commonly evaluated using the Hypervolume (HV) indicator, also called S-metric.

Definition 1.3. [6] The *Hypervolume indicator* $HV(\mathcal{P}(X)|r)$ is the M -dimensional Lebesgue measure λ_M of the region dominated by $\mathcal{P}(X)$ and bounded from below by a reference point $r \in \mathbb{R}^M$.

A feasible reference point is usually derived from domain knowledge of the problem. Multiple PFs can be compared by their HV if they were calculated with the same reference point and if they share the same objective values.

A common way of addressing MOOpt is by evolutionary algorithms like NSGA-II [7]. However, these algorithms have a high sample complexity reducing their effectiveness under a small number of evaluations n . As a tradeoff, Bayesian Optimization (BO) is a strategy to efficiently optimize MOOpt with expensive objective functions, aiming at minimizing the number of required evaluations. It treats the objective functions as black-boxes and places a prior over them, thereby capturing beliefs about their behaviour. Over time, as new samples are collected, the prior is updated iteratively to form the posterior distribution over the objective functions, usually with a Gaussian Process (GP). The posterior, in turn, is used in each iteration to determine the next sample-point to evaluate by employing an acquisition function as a heuristic to quantize the "usefulness" of the sample. Traditionally, the acquisition function is also responsible for balancing the exploration and exploitation tradeoff. Furthermore, for multiple objectives it is common to scale and accumulate the objective values to form a single-objective problem [19, 30].

A commonly used acquisition function is the Expected Improvement (EI) [29]

$$EI(x) = \mathbb{E} \max(f(x) - f^*, 0) \quad (1)$$

where f^* is the objective value of the best observed sample so far. For a given Bayesian model the EI can be evaluated with an integral over the posterior distribution either analytically or by Monte-Carlo sampling [35], which allows to approximate the EI as

$$qEI(x) \approx \frac{1}{N} \sum_{i=1}^N \max\{\max(\xi_i - f^*, 0)\}, \xi_i \sim \mathbb{P}(f(x) | \mathcal{D}), \quad (2)$$

where q is the number of samples considered jointly and $\mathbb{P}(f(x) | \mathcal{D})$ is the posterior distribution of the function f at x given the data \mathcal{D} observed so far.

We provide a methodology that combines DNN compression using filter pruning [22] and weight quantization [10] with MOBOpt for microcontroller targets. This allows us to optimize DNNs, considering the objectives of top-1 accuracy, memory consumption, and FLOPS, using a Bayesian model while minimizing the number of expensive objective evaluations. Our optimization approach consists of two building blocks: (1) the multi-objective optimization loop and (2) the objective functions evaluator. The optimization loop iteratively proposes new sets of training, pruning and quantization related hyperparameters, using our novel solver until a termination condition is met. The trained DNN resulting from the use of each of the proposed sets of hyperparameters is then evaluated which results in a vector of values, one for each objective. We propose a novel solver using an ensemble of competing local parameterizable policies which are iteratively trained on the underlying surrogate model using an Augmented Random Search (ARS) [26] reinforcement learning (RL) agent. Our experiments show the effectiveness of our approach in finding optimal DNNs by comparing our strategy to other state of the art multi-objective optimization strategies for several use-cases. The obtained solutions can be directly deployed on common microcontrollers.

The rest of the paper is structured as follows. Sec. 2 discusses related work. Sec. 3 provides details about our RL-agent and how we integrate it into our MOBOpt DNN hyperparameter exploration process. We evaluate our approach in Sec. 4 on several public data sets with different types of neural networks (Sec. 4.2), and on a synthetic optimization problem (Sec. 4.3). Sec. 5 concludes.

2 Related Work

Different approaches for efficient DNN design and optimization have been prominently discussed in scientific research: Dedicated architectures such as the MobileNet class [14, 32, 13] have been proposed, introducing scaling parameters and specialized layers, i.e., depthwise-separable convolutions, to control size and inference time. Neural Architecture Search (NAS) focuses on finding DNNs with optimal layer configurations related to a set of target metrics either by using RL [37] or by relaxing the problem to be differentiable and then using gradient-based methods [25]. Deep Compression features a number of techniques, including pruning [22], which dynamically removes weights during training, and weight quantization [17], which reduces the resolution at which weights are represented.

Based on these approaches, several deployment pipelines for embedded devices have been proposed: Han et al. [11] describe a pipeline combining network pruning, weight quantization and Huffman coding. Follow-up work compares different pruning and quantization methods [8]. Other pipelines are MCUNet [24] and Once-for-All [5] which both focus on NAS to find candidates for deployment.

Finding optimal hyperparameters for DNN training requires expertise and extensive trial and error. By considering DNN compression and deployment in a resource- and execution-time-constrained environment, additional tunable parameters for compression, as well as additional constraints are introduced that make the optimization problem a tradeoff between multiple objectives.

In scientific research, multi objective optimization (MOOpt) is a well established approach to solve problems with conflicting objectives. Some of the most thoroughly explored algorithms are based on multi-objective evolutionary algorithms (MOEA), e.g., NSGA-II [7]. Probably closest to our application, Wang et al. [33] explore hyperparameter and compression-parameter optimization using evolutionary algorithms for DNN deployment in combination with pruning and quantization. However, due to the population-based nature of evolutionary algorithms, MOEAs typically require a large number of evaluations, which in the case of DNN hyperparameter optimization can become time- and resource-consuming as a large set of networks have to be trained and evaluated.

As an alternative to MOEAs, algorithms based on Bayesian Optimization (BO) [29] have been used for MOOpt to minimize the number of function evaluations by utilizing surrogate models for each objective. A prominent representative of this Multi-Objective Bayesian Optimization (MOBOpt) class of algorithms is ParEGO [19], which randomly scales the MOOpt to single-target problems and then selects a sample based on the maximum expected improvement. Another recently proposed extension of this approach which specifically aims to tackle problems with a high-dimensional search spaces suggests employing locally modeled trust regions over subsets of the complete search space [9, 6].

Combining MOOpt with RL has also been explored: Moffaert et al. [28] propose a multi-policy RL algorithm that learns Pareto-dominating policies using Q-learning. There is also work that shows that MOOpt can be solved using Deep RL [23, 18]. Compared to our work, these approaches do not utilize Bayesian Optimization (BO) but instead directly apply RL to the objective function of the MOOpt problem. For our optimization problem this is problematic as evaluating our objective function, i.e., training a DNN, typically takes a significant amount of time. Furthermore, complex RL strategies like Q-learning or DRL introduce significant overhead to the sampling strategy. Instead, we propose to train a set of competing policies within MOBOpt that implement candidate sampling using very simplistic Augmented Random Search (ARS) [26] RL agents. To the best of our knowledge, we are the first to consider the combination of MOBOpt with RL to solve the specific problem of optimizing hyper- and compression parameters of DNNs targeting embedded microcontrollers.

3 Method

We first evaluated multiobjective hyperparameter optimization considering three well-known Bayesian optimization strategies, namely ParEgo [19], TurBO [9], and MorBO [6]. However, initial tests yielded ambivalent results across different seeds and use cases. After analyzing these optimization strategies using an artificial two-dimensional optimization problem, which we will discuss in more detail in Section 4.3, we decided to (a) adapt our EI implementation to not clamp "negative improvement" to zero, but instead penalize it by an additional hyperparameter (which we set to $1e^{-3}$), and (b) implement an ARS-based RL agent as our solver, with the goal of better understanding and exploiting the knowledge encoded by our Bayesian surrogate model.

Algorithm 1 Multi-Objective Bayesian Optimization with Augmented Random Search

Parameters: search budgeted J , learning rate α , directions sampled per iteration N , rollout horizon H , constant exploration noise v , number of top-performing directions to use k , number of objectives n , number of parameters p , number of ARS agents L , objective function $f(x) = [f_1(x), \dots, f_n(x)]$

Create initial prior by evaluating $f(x)$ several times using Latin-Hypercube sampling

for $i \leftarrow 1$ **to** J **do**

Fit Gaussian Process (GP) by maximising the marginal likelihood of previous evaluations of $f(x)$.

Select $\{x_1, x_2, \dots, x_L\}$ initial states from \mathcal{P}_{feas} of previous evaluations using k-means clustering.

repeat

for $l \leftarrow 0$ **to** L **do**

Sample directions $\varphi_1, \varphi_2, \dots, \varphi_N \in \mathbb{R}^{p \times n}$ with i.i.d. standard normal entries.

Collect the summed reward of the MC-sampled and scaled posteriors, see Equations 7 and 8, of $2N$ rollouts over the horizon H from the GP using local policy π_l and initial state x_l .

$$\pi_{l,j,k,+}(x) = (\theta_{l,j} + v\varphi_k)x \quad (3)$$

$$\pi_{l,j,k,-}(x) = (\theta_{l,j} - v\varphi_k)x \quad (4)$$

$$\pi_{l,j}(x) = \theta_{l,j}x \quad (5)$$

for $k \in \{1, 2, \dots, N\}$.

Sort the directions k by $\max\{r(\pi_{l,j,k,+}), r(\pi_{l,j,k,-})\}$, denote by φ_k the k -th largest direction, and by $r(\pi_{l,j,k,+})$ and $r(\pi_{l,j,k,-})$, the corresponding rewards.

Update the parameters θ_l of policy π_l using the top- k performing rollouts (with $\theta_{l,0} = 0$)

$$\theta_{l,j+1} = \theta_{l,j} + \frac{\alpha}{b\sigma_R} \sum_{k=1}^b (r(\pi_{l,j,k,+}) - r(\pi_{l,j,k,-}))\varphi_k \quad (6)$$

where σ_R is the standard deviation of the rewards used in the update step.

end for

until ARS termination condition is satisfied

Perform rollouts for all initial states $x_l \in \mathcal{P}_{feas}$ using policy π_l . For each π_l select the rollout yielding the highest reward and evaluate using $f(x)$ and extend the prior with the new evaluation

end for

To iteratively find new sets of hyperparameters, our optimization process uses an ensemble of competing multi-layer perceptron (MLP)-based RL agents, in particular ARS, as a replacement for traditional solvers such as NSGA-II or ParEGO. The policies consist of two linear layers with a hidden layer size of 64 resulting in a couple of thousand trainable parameters each. Augmented Random Search is an RL agent which learns a set of linear (or MLP) policies π_θ , parameterized by a set of vectors θ , one for each layer, for controlling a dynamic environment \mathbb{E}_ξ , with ξ encoding the randomness of the environment, maximizing/minimizing an average reward/loss $r(\pi_\theta, \xi)$. ARS achieves this by optimizing over the set of parameters θ by utilizing derivative-free optimization with noisy function evaluations and for each layer iteratively performing updates using directions of the form $\frac{r(\pi_{\theta+\nu\varphi, \xi_1}) - r(\pi_{\theta-\nu\varphi, \xi_2})}{\nu}$ for two i.i.d. random variables ξ_1 and ξ_2 , ν a positive real number (0.008 in our case), and φ a zero mean Gaussian vector with i.i.d. standard normal entries. The two rewards $r(\pi_{\theta+\nu\varphi, \xi_1})$ and $r(\pi_{\theta-\nu\varphi, \xi_2})$ are obtained by collecting two sets of trajectory rollouts from the system of interest in opposing directions. The authors highlight three aspects of their ARS agent: (1) Scaling the update by the standard deviation σ_R of the $2N$ rewards collected at each iteration to prevent harmful variations in the size of each update step, (2) normalizing the states to ensure that the policy weights the different components of the states equally, and (3) considering only the best-performing directions for the updates, which intuitively ensures that they occur over directions that have received high rewards.

We initialize the training of our competing ARS agents with different samples from the current feasible Pareto front. To find the most diverse set of samples, we perform k-means clustering on the

front if it consists of more elements than we can train policies. To query the objective values, i.e., accuracy, memory consumption, and FLOPS, for a proposed set of hyperparameters of a given DNN architecture, our objective function evaluator first trains, prunes, and quantizes the DNN. Afterwards, the DNN is converted into source code using an automatic code generator to accurately assess memory usage of weights and activation tensors. Our implementation performs this procedure using the compression and deployment pipeline proposed in [8]. The authors describe a configurable pipeline that supports both DNN pruning and full weight quantization. Following their results, we focus our experiments on iterative filter pruning and post-training static quantization.

We integrated ARS into MOBOpt as a parameterized, trainable solver, which can thus be seen as an alternative to traditional Bayesian solvers like ParEGO, see Algorithm 1. Compared to other Bayesian solvers, ARS’s derivative approach does not rely on second order partial derivatives (Hessian) and is therefore much less computationally complex. In addition, its random sampling approach is highly parallelizable, allowing for efficient GPU-accelerated execution.

We define the states x_0, x_1, \dots, x_L of our L competing agents as vectors of the parameters of the search space of our optimization problem. Each agent performs actions based on its trainable policy π_θ by altering the parameter values of its state vector within given bounds. We train the competing policies of our ARS agents for each sample after evaluating the objective function by performing rollouts on posteriors sampled from the GP which we fitted by maximising the marginal likelihood of previously queried evaluation of the objective function beforehand, compare [34]. The policy training performed for each sample ends after a maximum number of training steps has been conducted. To obtain the initial prior for the GP, we propose candidates during the first couple of iterations of the optimization using Latin Hypercube sampling [27]. We chose this approach over random sampling because we found that by using Latin Hypercube sampling, we could significantly improve the expressiveness of our priors and therefore enhance the performance of all evaluated GP-based sampling strategies.

As a reward $r(x)$, we first scale our $n = 4$ objectives to a single objective value using augmented Chebyshev scalarization [19], see Equation (7), where $\rho = 0.005$ is a small positive value and λ is a weight vector that we draw uniformly at random at the beginning of each sample. We then calculate the difference between the scaled objective and the best previously visited (scaled) objective f^* as the reward that the ARS agents maximize, see Equation (8).

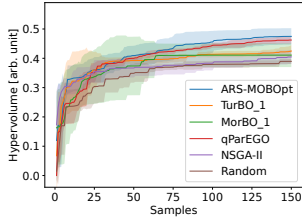
$$f_\lambda(x) = \max_{j=1}^n (\lambda_j f_j(x)) + \rho \sum_{j=1}^n \lambda_j f_j(x) \quad (7)$$

$$r(x) = \begin{cases} f_\lambda(x) - f_\lambda(f^*), & \text{if } (f_\lambda(x) - f_\lambda(f^*)) > 0 \\ 1e^{-3}(f_\lambda(x) - f_\lambda(f^*)), & \text{otherwise} \end{cases} \quad (8)$$

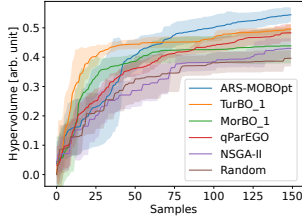
To avoid having to compute the expected value over the posterior of the GP when computing the acquisition function, a common approach is to use Monte-Carlo (MC) sampling as an approximation to evaluating the integral over the posterior distribution. In our case, we implement a quasi-MC sampling approach to estimate the reward used to train the ARS agents with a fixed set of base samples.

As a result, the reward $r(x)$ used by our ARS agents is comparable to acquisition functions used in traditional Bayesian optimization. In particular, our approach is similar to the expected improvement (EI) used by ParEgo, with the notable difference that we consider penalized "negative improvements" instead of clamping it to zero. The main reason for clamping "negative improvement" in combination with a Monte Carlo-based evaluation of the GPs is to increase the attractiveness of regions with high uncertainty, and is therefore the mechanism of EI to control the tradeoff between exploration and exploitation. However, we argue that we can still achieve the desired tradeoff if we instead penalize "negative improvements" by multiplication with a small constant factor, while allowing our ARS policies to learn from situations where the current objective function evaluation is worse than the best previously visited one.

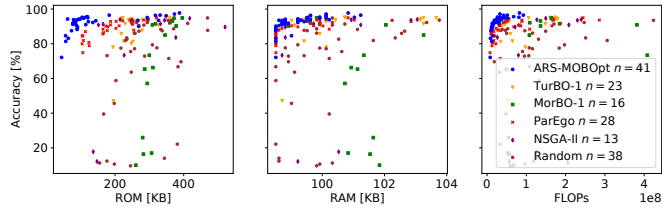
After training the competing ARS agents, we perform several rollouts for each of them starting from their respective starting points selected from $\mathcal{P}_{feas}(X)$. We then select the policy that yielded the overall best reward to propose the next set of hyperparameters to be evaluated on the objective function in the next sample. A variant of this approach would be to consider a set of best-performing parametrizations as candidates for a batched optimization in different segments of the Pareto front.



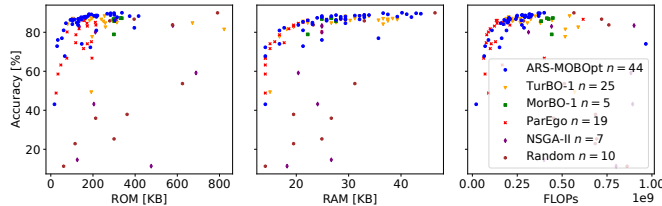
(a) MobileNetv3, DaLiAc.



(b) ResNet, CIFAR10.



(a) MobileNetv3, DaLiAc.



(b) ResNet, CIFAR10.

Figure 1: Our approach (ARS-MOBOpt) outperformed all other optimization strategies.

Figure 2: Feasible Pareto sets proposed by our RL-based MOBOpt of DNNs (blue) compared to other Bayesian and evolutionary approaches. In both cases we find samples dominating those proposed by the other algorithms while meeting imposed target constraints ($<1\text{MB}$ ROM, $<256\text{KB}$ RAM, $<1e^9$ FLOPs).

4 Evaluation

We applied our multi-objective DNN hyperparameter optimization on two use-cases with 150 samples each: (1) Classification of 32×32 RGB images (CIFAR10 dataset [20]), trained with a reduced version of ResNet18 [12] (only three residual blocks instead of four, 1.6M initial parameters) and (2) Time series classification of (daily) human activities (DaLiAc) [21] with a window length of 1024 datapoints, trained with a scaled down version of MobileNetv3 [13] (2.8M initial parameters). Compared to models commonly used by relevant benchmarks for embedded AI, e.g., TinyML Perf [4], we did not decrease the initial numbers of neurons in our DNNs’ trainable layers as our optimization process uses pruning and therefore dynamically adjusts the exact number of neurons during training. We trained our models using Stochastic Gradient Decent (SGD) and exponential learning rate decay. For the optimization, we assumed 256 KB of RAM, 1 MB of ROM and $1e^9$ FLOPs as constraints imposed by common microcontroller platforms.

The detailed list of hyperparameters considered by our optimizer and their continuous sampling intervals derived from expert knowledge can be found in the supplementary material. We consider seven parameters controlling general properties of DNN training (training length, batch size, properties of the optimizer and learning rate) and four that control the filter pruning. We use the automated gradual pruning algorithm [36] to generate our pruning schedule. It takes a start and end epoch calculated relatively to the number of training epochs and a number of iterative steps as an input. Our optimization considers the pruning sparsity hyperparameter, i.e., how many filters are removed, for each convolutional layer separately. Therefore, the search space considered increases with the depth of the optimized DNN as for each prunable layer an additional pruning sparsity parameter is added which means that the search space is extended by one dimension.

4.1 Algorithmic Benchmark

As our first experiment we compared the quality of our approach (ARS-MOBOpt) to several well-known Bayesian optimization strategies (ParEGO [19], TurBO [9], MorBO [6]), one evolutionary approach (NSGA-II [7]) and a random sampling approach as a baseline, see Fig. 1. We gave each optimization strategy a search budget of 150 samples to evaluate the objective functions and monitored the improvement of the feasible hypervolume over the samples. For all tested Bayesian strategies the first 10 samples were conducted as priors using Latin Hypercube sampling [27]. We normalized our objectives accuracy, ROM consumption, RAM consumption and FLOPs to their respective constraints and used the maximum feasible objective value as a common reference when computing

Table 1: Excerpt from the results of the multivariate datasets of the UEA & UCR time series classification benchmark [2] for our ARS strategy (columns 3–7) and ParEGO (columns 8–12). For both strategies, we show the achieved hypervolume after 150 trials as well as the maximum accuracy. We also show the minimum memory and FLOPs required to achieve at least 70% accuracy.

Dataset	InceptionTime Acc. [%]	ARS					ParEGO				
		HV	Acc. [%]	ROM [Kb]	RAM [Kb]	FLOPs	HV	Acc. [%]	ROM [Kb]	RAM [Kb]	FLOPs
Epilepsy	98.55	0.97	97.81	1.21×10^5	4.92×10^3	3.57×10^6	0.93	94.16	6.70×10^4	3.39×10^3	2.05×10^6
BasicMotions	100.00	0.96	97.50	1.31×10^5	3.00×10^3	2.75×10^6	0.97	97.50	8.67×10^4	2.50×10^3	1.49×10^6
Cricket	98.61	0.96	97.22	1.00×10^5	2.99×10^4	1.60×10^7	0.95	95.83	7.61×10^4	3.05×10^4	1.01×10^7
ERing	87.78	0.96	96.67	1.00×10^5	1.99×10^3	2.03×10^6	0.93	93.33	7.32×10^4	1.23×10^3	1.00×10^6
ArticularyWordRecognition	98.33	0.94	95.64	1.51×10^5	6.18×10^3	4.19×10^6	0.92	92.36	8.07×10^4	5.33×10^3	2.13×10^6
UWaveGestureLibrary	87.81	0.91	91.67	1.10×10^5	6.94×10^3	5.78×10^6	0.91	91.67	7.21×10^4	4.09×10^3	3.03×10^6
NATOPS	96.11	0.86	87.22	1.29×10^5	5.78×10^3	2.79×10^6	0.78	78.33	1.00×10^5	4.94×10^3	1.12×10^6
SelfRegulationSCP1	83.96	0.79	79.85	1.05×10^5	2.24×10^4	1.78×10^7	0.78	78.73	7.81×10^4	2.24×10^4	7.15×10^6
PEMS-SF	–	0.76	81.50	1.38×10^5	5.55×10^5	7.98×10^6	0.79	84.97	2.38×10^5	5.56×10^3	5.72×10^7
Heartbeat	58.05	0.73	74.51	8.16×10^4	9.92×10^4	8.14×10^6	0.73	74.02	6.25×10^4	9.92×10^4	2.79×10^6

the hypervolume. Furthermore, we performed 5 independent seeds for each strategy and provide the observed variance in Fig. 1 as well.

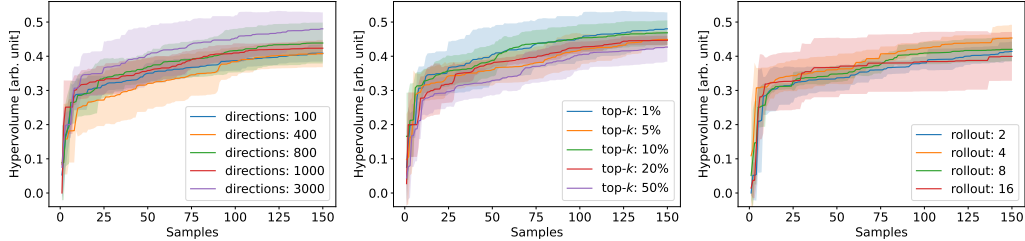
We share results for two common DNN architectures, MobileNetv3 and ResNet18, which we trained using two datasets, DaLiAc and CIFAR10, see Fig. 1a and Fig. 1b. The plots show the observed hypervolume over the number of optimization samples. Therefore, the resulting curves, one for each optimization strategy, describe the improvement of the hypervolume. First, all informed solvers outperformed the independent random sampling baseline for both use-cases. Second, all the approaches that are based on Bayesian optimization, i.e., TurBO, MorBO, ParEGO and ARS-MPBOpt, which consider the constraints of a very tight search budget of 150 samples, performed better than the evolutionary sampling strategy (NSGA-II). Additionally, for both use-cases a significant Hypervolume improvement can be observed when using our ARS-based sampling strategy with 3000 sampling directions, a top- k selection percentage of 1%, and a rollout horizon of 4 to train the competing policies. We interpret this to mean that by using a trainable RL-based strategy to determine new promising parametrizations as the optimization progresses, our algorithm makes much better use of the knowledge about the search space encoded in the surrogate model than the other non-trainable Bayesian sampling approaches.

In addition, we provide qualitative results for both considered use cases, see Fig. 2. The plots show the Pareto optimal samples for our approach (in blue) compared to all other algorithms tested, see Fig. 2a and Fig. 2b. For both use cases, ARS-MOBOpt was able to find samples that are Pareto-dominant over those proposed by the other algorithms, while satisfying all imposed target constraints ($<1\text{MB}$ ROM, $<256\text{KB}$ RAM, $<1\text{e}9$ FLOPs). Moreover, for both use cases, the number of elements n in the two sets of feasible Pareto optimal configurations resulting from our approach are larger than the sets found by the other approaches, implying that our algorithm was able to provide a significantly larger variety of Pareto optimal samples (deployable DNNs).

To get more insight into the general performance of ARS, we tested it on a subset of the multivariate datasets of the UEA & UCR time series classification benchmark [2] and compared ourselves to ParEGO using the same setup as described above, see Table 1 for all data sets on which reasonable models with a predictive accuracy of at least 70% are found (and the supplementary material for a complete listing). To provide context, we also list reference results for InceptionTime [16], that we took from [2]. We let both ARS and ParEGO optimize a CNN architecture with a single regular convolution followed by 10 depth-wise separable convolutions with batchnorm and with a total of 5 squeeze and excitation blocks [15] after convolutions 10, 8, 6, 4, and 2, followed by adaptive average pooling and a single linear layer for classification (2.6m initial parameters). Our approach achieves a better hypervolume than ParEGO in 7 of 10 data sets (and is en par on one data set). If we also consider data sets where we found models with predictive accuracies below 70% our approach outperforms ParEGO in approx. two-thirds of the data sets, see supplementary material. From the results we also see that compared to ParEGO, our algorithm was generally better at finding DNNs with higher accuracy scores, but often at the cost of slightly higher memory and FLOPs requirements.

4.2 Robustness and Hyperparameter Selection

Our proposed ARS sampling strategy can be configured with a number of hyperparameters that affect the behavior of the ARS algorithm, see Alg. 1. The quality of the results obtained by our algorithm can vary depending on the parameterization, see Fig. 3: In general, choosing a learning rate



(a) Number of *sampling directions* N performed for each step. (b) Percentage of *top-k* performing samples from N selected for policy updates. (c) *Rollout Horizon* H performed by the competing policies.

Figure 3: Detailed results examining the effects of the three key ARS hyperparameters on the achieved hypervolume, 5 seeds each. MobileNetV3, 1.6M init. params, DaLiAc dataset, window length 1024.

of $1e^{-3}$, an exploration noise of $1e^{-2}$, a top- k selection rate of 1%, a number of sampling directions between 400 and 3000, and a rollout horizon of 4 yielded the best results. In the following, we want to further discuss the impact of key hyperparameters, i.e., the number of sampling directions N , the top- k percentage of directions selected for policy updates, and the number of steps H taken for each episode (rollout horizon), to provide a broader understanding of their effects.

First, especially for complex optimization problems with a high-dimensional parameter space, a high number of sampling directions significantly improved the hypervolume that our ARS-based sampling strategy was able to achieve, compared to a low number of directions, which often resulted in a below-average performance, see Fig. 3a. However, we also found, that it is not feasible to increase the number of directions indefinitely to support more and more complex problems, as this also significantly increases the time required to train the ARS policies and the memory consumption of our algorithm. We found that the exact number of sampling directions which is required to obtain a competitive result is highly correlated with the complexity of the underlying optimization problem.

Second, when increasing the top- k percentage of sampling directions selected by ARS to perform policy updates, we observed that only selecting a small subset of 1% of the sampled directions to perform policy updates improved the hypervolume achieved by ARS compared to using larger subsets, see Fig. 3b. Our observation is thus consistent with [26]’s argument for introducing the hyperparameter as part of ARS. The authors point out that including all observed rewards in the parameter update can be detrimental to performance because outliers can easily introduce bias.

Last, we found that an optimal episode length (rollout horizon) is at $H = 4$ steps, see Fig. 3c. Both a significantly smaller and larger episode length on average resulted in a decreased performance. Still, we want to point out that we observed a significantly larger variance for longer episode lengths compared to shorter episode lengths. We interpret this to mean that even though ARS can perform excellent at longer episode lengths in some cases, especially at a lower number of samples < 100 , this seems to make the algorithm more unstable overall and thus less reliable.

4.3 Intuition

To better understand why our RL-based solver can improve on other Bayesian solvers like ParEgo, we analyzed both using a synthetic optimization problem. Suppose we minimize a two-dimensional single objective optimization problem [31] using both ParEgo and our approach, see Fig. 4. We chose this problem because it presents an interesting challenge: it has a landscape with large areas with little to no gradient combined with some steep minima and maxima. We provide the topography of the objective function in Fig. 4e and show the respective Bayesian surrogates of ParEgo and ARS-MOBOpt as well as the topographies of their expected improvement (EI) after 40 trials in Fig. 4 and 5. For our approach (ARS-MOBOpt), we also visualize the rollouts performed during the validation of the local policies for five selected start points (red crosses) after the last (40th) sample.

We manually selected two sets of priors (marked as red triangles) to provide both algorithms with interesting starting situations: First, a situation where all samples are close together in a region with almost no gradient, see Fig. 4a and 5a. This initialization is interesting because it provides almost no information about the environment, requiring extensive exploration by the algorithms before they can exploit found minima. Second, a more general starting situation with a broader distribution of prior

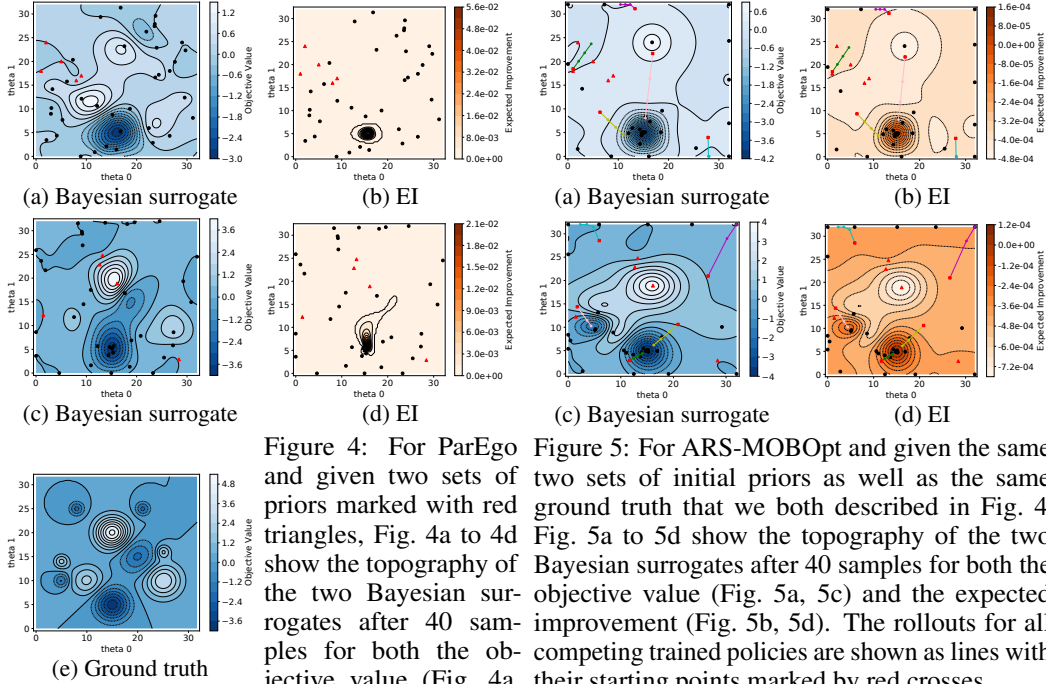


Figure 4: For ParEgo and given two sets of initial priors marked with red triangles, Fig. 4a to 4d show the topography of the two Bayesian surrogates after 40 samples for both the objective value (Fig. 4a, 4c) and the expected improvement (Fig. 4b, 4d) (Ground truth depicted in Fig. 4e [31] and the global minimum is at $\theta_0 = 15$ and $\theta_1 = 5$).

samples, see Fig. 4c and 5c. This initialization focuses more on evaluating how well the algorithms can apply the exploration-exploitation tradeoff and how fast they can find minima. For both priors, we took care not to include samples close to the global minimum.

Looking at the results proposed by ParEgo (marked as black dots) after 40 samples in Fig. 4, it is clear that for both sets of priors the algorithm seems to have had a clear focus on exploration, leading to a wide sampling of the search space. However, looking at Fig. 4a, this can lead to situations where even though the global optimum has been found it was not fully exploited. Furthermore, we argue that this focus on exploration is mainly a result of the definition of the EI as it does not consider any "negative improvement". Looking at Figs. 4d and 4b, it is clear that this can result in large parts of the acquisition function having no gradient. We argue that this is not optimal when relying on gradient-based solvers, as the ParEgo implementation typically does.

In comparison, if we look at the result of our proposed ARS-based approach in Fig. 5, it is clear that our competing local policies, visualized as lines with red crosses as their starting point, have become experts in solving the environment around their starting point and can therefore provide sound solutions even in regions without significant gradients. Therefore, compared to ParEgo, we observed less undirected exploration and a clearer focus on exploiting environmental knowledge, compare e.g. Fig. 5a and Fig. 4a. However, despite this more pronounced focus on exploitation, our solver was still able to escape local minima when it fell into one, see Fig. 5c.

5 Conclusion

We presented a methodology for efficient multi-objective DNN optimization based on Bayesian optimization and Augmented Random Search (ARS) for microcontroller targets. Since the objectives accuracy, ROM consumption, RAM consumption and FLOPs were expensive to evaluate and we were faced with a limited search budget, we focused on performing time-efficient optimization of both DNN hyper- and compression-parameters to enable an optimal deployment on microcontroller platforms. We provided results for two different problems considering two datasets and DNN

architectures and showed empirically that our algorithm was able to yield a better feasible Pareto front compared to well-known Bayesian optimization strategies like ParEGO, TurBO or MorBO as well as evolutionary algorithms like NSGA-II.

References

- [1] T. Akiba, S. Sano, T. Yanase, T. Ohta, and M. Koyama. Optuna: A Next-generation Hyperparameter Optimization Framework. *KDD '19*, 2019.
- [2] A. Bagnall, J. Lines, A. Bostrom, J. Large, and E. Keogh. The great time series classification bake off: a review and experimental evaluation of recent algorithmic advances. *Data Mining and Knowledge Discovery*, 31:606–660, 2017.
- [3] M. Balandat, B. Karrer, D. Jiang, S. Daulton, B. Letham, A. G. Wilson, and E. Bakshy. BoTorch: A Framework for Efficient Monte-Carlo Bayesian Optimization. *Conference on Neural Information Processing Systems (NeurIPS)*, 2020.
- [4] C. Banbury, V. J. Reddi, P. Torelli, J. Holleman, N. Jeffries, C. Kiraly, P. Montino, D. Kanter, S. Ahmed, D. Pau, et al. Mlperf tiny benchmark. *Conference on Neural Information Processing Systems (NeurIPS)*, 2021.
- [5] H. Cai, C. Gan, T. Wang, Z. Zhang, and S. Han. Once-for-all: Train one network and specialize it for efficient deployment. In *International Conference on Learning Representations*, 2020.
- [6] S. Daulton, D. Eriksson, M. Balandat, and E. Bakshy. Multi-objective bayesian optimization over high-dimensional search spaces. In *The 38th Conference on Uncertainty in Artificial Intelligence*, 2022.
- [7] K. Deb, A. Pratap, S. Agarwal, and T. Meyarivan. A fast and elitist multiobjective genetic algorithm: Nsga-II. *IEEE Transactions on Evolutionary Computation*, 6(2):182–197, 2002.
- [8] M. Deutel, P. Woller, C. Mutschler, and J. Teich. Deployment of Energy-Efficient Deep Learning Models on Cortex-M based Microcontrollers using Deep Compression. *arXiv:2205.10369*, 2022.
- [9] D. Eriksson, M. Pearce, J. R. Gardner, R. Turner, and M. Poloczek. Scalable global optimization via local bayesian optimization. In *Proceedings of the 33rd International Conference on Neural Information Processing Systems (NeurIPS)*, 2019.
- [10] A. Gholami, S. Kim, Z. Dong, Z. Yao, M. W. Mahoney, and K. Keutzer. A survey of quantization methods for efficient neural network inference. *arXiv:2103.13630*, 2021.
- [11] S. Han, H. Mao, and W. J. Dally. Deep compression: Compressing deep neural networks with pruning, trained quantization and huffman coding. *International Conference on Learning Representations*, 2016.
- [12] K. He, X. Zhang, S. Ren, and J. Sun. Deep residual learning for image recognition. In *IEEE Conference on Computer Vision and Pattern Recognition (CVPR)*, pages 770–778, 06 2016.
- [13] A. Howard, M. Sandler, G. Chu, L.-C. Chen, B. Chen, M. Tan, W. Wang, Y. Zhu, R. Pang, V. Vasudevan, Q. V. Le, and H. Adam. Searching for mobilenetv3. *arXiv:1905.02244*, 2019.
- [14] A. G. Howard, M. Zhu, B. Chen, D. Kalenichenko, W. Wang, T. Weyand, M. Andreetto, and H. Adam. Mobilenets: Efficient convolutional neural networks for mobile vision applications. *arXiv:1704.04861*, 2017.
- [15] J. Hu, L. Shen, and G. Sun. Squeeze-and-excitation networks. In *IEEE/CVF Conference on Computer Vision and Pattern Recognition*, pages 7132–7141, 2018.
- [16] H. Ismail Fawaz, B. Lucas, G. Forestier, C. Pelletier, D. F. Schmidt, J. Weber, G. I. Webb, L. Idoumghar, P.-A. Muller, and F. Petitjean. Inceptiontime: Finding alexnet for time series classification. *Data Mining and Knowledge Discovery*, 34:1936–1962, 2020.
- [17] B. Jacob, S. Kligys, B. Chen, M. Zhu, M. Tang, A. Howard, H. Adam, and D. Kalenichenko. Quantization and training of neural networks for efficient integer-arithmetic-only inference. *IEEE Conference on Computer Vision and Pattern Recognition (CVPR)*, 2018.
- [18] S. Kim, I. Kim, and D. You. Multi-condition multi-objective optimization using deep reinforcement learning. *Journal of Computational Physics*, 462:111263, 2022.

- [19] J. Knowles. Parego: a hybrid algorithm with on-line landscape approximation for expensive multiobjective optimization problems. *IEEE Transactions on Evolutionary Computation*, 10(1):50–66, 2006.
- [20] A. Krizhevsky. Learning Multiple Layers of Features from Tiny Images. *University of Toronto*, 2012.
- [21] H. Leutheuser, D. Schuldhaus, and B. M. Eskofier. Hierarchical, multi-sensor based classification of daily life activities: comparison with state-of-the-art algorithms using a benchmark dataset. *PloS one*, 8(10):e75196, 2013.
- [22] H. Li, A. Kadav, I. Durdanovic, H. Samet, and H. P. Graf. Pruning Filters for Efficient ConvNets. *arXiv:1608.08710*, 2017.
- [23] K. Li, T. Zhang, and R. Wang. Deep reinforcement learning for multiobjective optimization. *IEEE transactions on cybernetics*, 51(6):3103–3114, 2020.
- [24] J. Lin, W.-M. Chen, Y. Lin, j. cohn, C. Gan, and S. Han. MCUNet: Tiny Deep Learning on IoT Devices. *Conference on Neural Information Processing Systems (NeurIPS)*, 2020.
- [25] H. Liu, K. Simonyan, and Y. Yang. DARTS: Differentiable architecture search. In *International Conference on Learning Representations*, 2019.
- [26] H. Mania, A. Guy, and B. Recht. Simple random search of static linear policies is competitive for reinforcement learning. In *Advances in Neural Information Processing Systems (NeurIPS)*, 2018.
- [27] M. D. McKay, R. J. Beckman, and W. J. Conover. A comparison of three methods for selecting values of input variables in the analysis of output from a computer code. *Technometrics*, 42(1):55–61, 2000.
- [28] K. V. Moffaert and A. Nowé. Multi-objective reinforcement learning using sets of pareto dominating policies. *Journal of Machine Learning Research*, 15(107):3663–3692, 2014.
- [29] J. Moćkus. On bayesian methods for seeking the extremum. In *Optimization Techniques IFIP Technical Conference*, pages 400–404, 1975.
- [30] B. Paria, K. Kandasamy, and B. Póczos. A flexible framework for multi-objective bayesian optimization using random scalarizations. In *Uncertainty in Artificial Intelligence*, pages 766–776. PMLR, 2020.
- [31] K. M. Passino. *Biomimicry for optimization, control, and automation*. Springer Science & Business Media, 2005.
- [32] M. Sandler, A. Howard, M. Zhu, A. Zhmoginov, and L.-C. Chen. Mobilenetv2: Inverted residuals and linear bottlenecks. In *2018 IEEE/CVF Conference on Computer Vision and Pattern Recognition*, pages 4510–4520, 2018.
- [33] Z. Wang, T. Luo, M. Li, J. T. Zhou, R. S. M. Goh, and L. Zhen. Evolutionary multi-objective model compression for deep neural networks. *IEEE Computational Intelligence Magazine*, 16(3):10–21, 2021.
- [34] C. Williams and C. Rasmussen. Gaussian processes for regression. In D. Touretzky, M. Mozer, and M. Hasselmo, editors, *Advances in Neural Information Processing Systems (NeurIPS)*, volume 8. MIT Press, 1995.
- [35] J. T. Wilson, R. Moriconi, F. Hutter, and M. P. Deisenroth. The reparameterization trick for acquisition functions. *NIPS 2017 Workshop on Bayesian Optimization (BayesOpt 2017)*, 2017.
- [36] M. Zhu and S. Gupta. To prune, or not to prune: exploring the efficacy of pruning for model compression. *arXiv:1710.01878*, 2017.
- [37] B. Zoph and Q. Le. Neural architecture search with reinforcement learning. In *International Conference on Learning Representations*, 2017.

6 Supplementary Material

6.1 Training Details & Optimization Variables

We present a multi-objective Bayesian optimization approach for DNN hyperparameter optimization that uses deep compression, i.e., pruning and quantization, to find feasible tradeoffs between DNN accuracy and resource consumption. Furthermore, we present a novel solver based on Augmented Random Search. An illustration of our process can be found in Fig. 6, with its implementation based on PyTorch, the Optuna [1] framework and BoTorch [3]. The implementation consists of two building blocks: (1) the multi-objective optimization loop marked in blue and (2) a set of objective function evaluators marked in orange, for which we use the implementation discussed in [8]. The optimization loop iteratively proposes new sets of hyperparameter configurations using ARS as its solver until a termination condition is met.

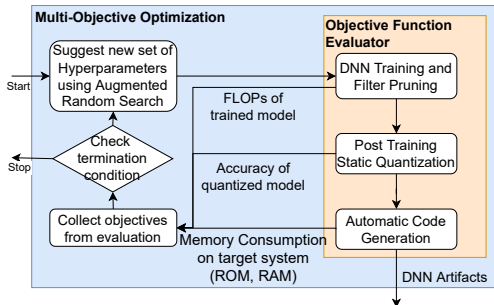


Figure 6: Overview of our proposed RL-based multi-objective Bayesian DNN hyperparameter optimization approach for microcontroller targets.

We provide a complete listing of the hyperparameters that are optimized and their search space intervals in Table 2. The first seven parameters are hyperparameters related to general DNN training, while the last five are related to compression. Note that each trainable layer (convolutions and linear layers) has its own optimizable pruning sparsity, and that we use iterative pruning with the pruning start and pruning end parameters defined relative to the number of training epochs. The search space intervals are chosen either based on expert knowledge, e.g., learning rate, momentum or weight decay, or based on time and hardware constraints of the optimization, e.g., training epochs and batch size.

Table 2: Hyperparameters considered by the multi-objective optimization. Learning rate schedule, pruning start, and end are relative to the epochs.

Parameter	Search Space	Interval
epochs	uniform	[100, 500]
batch size	uniform	[20, 200]
learning rate (lr)	log. uniform	$[1e^{-5}, 1e^{-2}]$
momentum	log. uniform	[0.7, 0.99]
lr schedule	uniform	[0.4, 0.9]
lr gamma	uniform	[0.4, 0.9]
weight decay	log. uniform	[0.6, 0.99]
pruning start	uniform	[0.0, 0.6]
pruning end	uniform	[0.8, 0.95]
pruning steps	uniform	[1, 20]
pruning sparsity	uniform	[0.1, 0.99]

6.2 Complete Listing for UEA & ICR Time Series Classification Benchmark

In Table 3 we provide all results we obtained for the multivariate datasets of the UEA & UCR time series classification benchmark [2]. We provide results for our ARS strategy (columns 3–7) and ParEGO (columns 8–12). For both strategies, we show the achieved hypervolume after 150 trials as well as the maximum accuracy. We also show the minimum memory and FLOPs required to achieve at least 70% accuracy. If no trained networks were found that met these requirements (marked in gray), we show the memory and FLOPs consumption of the network that achieved the highest accuracy. We provide single objective reference results for InceptionTime [16] as taken from [2].

Table 3: Results for the multivariate datasets of the UEA & UCR time series classification benchmark [2] for our ARS strategy (columns 3–7), ParEGO (columns 8–12) and InceptionTime (column 1) as a reference.

Dataset	InceptionTime		ARS				ParEGO				
	Acc. [%]	HV	Acc. [%]	ROM [Kb]	RAM [Kb]	FLOPs	HV	Acc. [%]	ROM [Kb]	RAM [Kb]	FLOPs
Epilepsy	98.55	0.97	97.81	1.21×10^5	4.92×10^3	3.57×10^6	0.93	94.16	6.70×10^4	3.39×10^3	2.05×10^6
BasicMotions	100.00	0.96	97.50	1.31×10^5	3.00×10^3	2.75×10^6	0.97	97.50	8.67×10^4	2.50×10^3	1.49×10^6
Cricket	98.61	0.96	97.22	1.00×10^5	2.99×10^4	1.60×10^7	0.95	95.83	7.61×10^4	3.05×10^4	1.01×10^7
ERing	87.78	0.96	96.67	1.00×10^5	1.99×10^3	2.03×10^6	0.93	93.33	7.32×10^4	1.23×10^3	1.00×10^6
ArticulatoryWordRecognition	98.33	0.94	95.64	1.51×10^5	6.18×10^3	4.19×10^6	0.92	92.36	8.07×10^4	5.33×10^3	2.13×10^6
UWaveGestureLibrary	87.81	0.91	91.67	1.10×10^5	6.94×10^3	5.78×10^6	0.91	91.67	7.21×10^4	4.09×10^3	3.03×10^6
NATOPS	96.11	0.86	87.22	1.29×10^5	5.78×10^3	2.79×10^6	0.78	78.33	1.00×10^5	4.94×10^3	1.12×10^6
SelfRegulationSCP1	83.96	0.79	79.85	1.05×10^5	2.24×10^4	1.78×10^7	0.78	78.73	7.81×10^4	2.24×10^4	7.15×10^6
PEMS-SF	–	0.76	81.50	1.38×10^5	5.55×10^5	7.98×10^6	0.79	84.97	2.38×10^5	5.56×10^5	5.72×10^7
Heartbeat	58.05	0.73	74.51	8.16×10^4	9.92×10^4	8.14×10^6	0.73	74.02	6.25×10^4	9.92×10^4	2.79×10^6
HandMovementDirection	36.49	0.60	60.81	1.71×10^5	2.36×10^4	1.01×10^7	0.45	45.95	9.95×10^4	1.86×10^4	9.72×10^6
FingerMovements	56.00	0.59	60.00	1.62×10^5	6.27×10^3	3.10×10^6	0.58	59.00	1.68×10^5	6.97×10^3	4.34×10^6
SelfRegulationSCP2	47.22	0.58	58.33	1.05×10^5	5.87×10^4	3.92×10^7	0.56	56.67	1.83×10^5	3.92×10^4	2.42×10^7
Handwriting	64.24	0.57	58.00	2.08×10^5	5.42×10^3	4.65×10^6	0.71	72.00	1.31×10^5	4.75×10^3	5.56×10^6
EigenWorms	–	0.55	60.16	2.11×10^5	4.50×10^5	5.47×10^8	0.50	53.91	1.42×10^5	6.83×10^5	7.03×10^8
MotorImagery	–	0.55	60.00	1.49×10^5	7.71×10^5	8.38×10^7	0.55	61.00	1.58×10^5	8.34×10^5	1.91×10^8
EthanolConcentration	23.19	0.53	54.02	1.47×10^5	5.90×10^4	4.71×10^7	0.49	49.43	2.09×10^5	4.55×10^4	6.47×10^7
AtrialFibrillation	20.00	0.53	53.33	1.47×10^5	2.15×10^4	1.76×10^7	0.59	60.00	2.03×10^5	1.68×10^4	3.14×10^7
StandWalkJump	40.00	0.49	50.00	2.01×10^5	9.37×10^4	5.98×10^7	0.66	66.67	2.10×10^5	8.62×10^4	1.44×10^8
DuckDuckGeese	–	0.39	46.00	1.74×10^5	1.45×10^6	3.40×10^7	0.34	40.00	1.44×10^5	1.45×10^6	1.44×10^7
PhonemeSpectra	–	0.21	21.42	2.16×10^5	1.52×10^4	8.70×10^6	0.19	19.49	1.78×10^5	1.24×10^4	1.02×10^7